Single-mode interband cascade laser with a slotted waveguide

J. Fordyce, D. Diaz-Thomas, L. O'Faolain, A. Baranov, T. Piwonski, L. Cerutti

Single-mode interband cascade laser with a slotted waveguide

J. A. M. Fordyce,[1,2,3] D. A. Diaz-Thomas,[1] L. O'Faolain,[2,3] A. N. Baranov,[1] T. Piwonski,[2,3] and L. Cerutti[1]
[1)] *IES, Univ. Montpellier, CNRS, F-34000 Montpellier, France*
[2)] *CAPPA, Munster Technology University, T12 P928 Cork, Ireland*
[3)] *Tyndall National Institute, T12 R5CP Cork, Ireland*

(*Electronic mail: laurent.cerutti@umontpellier.fr)

(Dated: 4 November 2022)

The design of a single-mode interband cascade laser (ICL) using a slotted waveguide is presented. This technique was explored as an inexpensive alternative to distributed feedback (DFB) lasers since standard photolithography can be used in fabrication and complex techniques like e-beam lithography, re-growth steps, and/or metal gratings can be avoided. The design of slotted waveguides must be carefully simulated before fabrication to ensure the efficacy of the photolithography masks with each ICL growth. Limitations and the behaviour of key design parameters are discussed. Single-mode emission was achieved for certain temperature and injected current conditions, validating the operation of an Sb based slotted laser. The slotted ICLs were emitting from a single longitudinal mode at 3.5 µm and 2 mW of power per facet output at 20 °C with threshold currents around 80 mA.

The market for technology that can detect small gas leaks in industrial plants is growing, and repairing even small leaks can greatly reduce their emission and improve the safety of the working environment. Laser absorption spectroscopy is a very sensitive, selective technique that requires adequate cost-effective sensors and sources. The 3 µm to 5 µm spectral band is of particular interest because of the absorption lines present from many different hydrocarbons and volatile organic compounds[1], like methane, carbon dioxide, or chloroform. These gases are major contributors to global warming, climate change[23] and/or are harmful to people.

Quartz-enhanced photoacoustic spectroscopy (QEPAS) detection schemes, for example, require a laser source with an appropriate wavelength and output power to excite the molecules and generate workable signals[4]. The laser must be single-mode and tunable with low power consumption and have a long lifetime to be used as a portable, packaged sensor.

ICLs are a good candidate for laser sources in the 3 µm to 5 µm wavelength range because of their low threshold currents and voltages in comparison to diode lasers or quantum cascade lasers (QCLs), who offer less efficient performance[567]. Additionally, ICLs can be grown on Si substrates and exhibit extremely long lifetimes at an extrapolated 300 000 h of operation[8].

Several types of ICLs based on loss coupling have recently demonstrated single-mode emission with side mode suppression ratios (SMSR) >20 dB[9]. These approaches are expensive because they require extensive e-beam lithography and incur losses from the metallic grating deposited on top or on both sides of the mesa which reduce the laser output power[101112]. Still, DFB ICLs are commercially available over the range 3 µm to 4 µm with output powers >5 mW in continuous wave (CW) operation at room temperature and offer ≈20 nm of wavelength tuning[9].

Single-mode operation can also be achieved with a few well-placed periodic defects in the waveguide of a Fabry-Pérot cavity[13]. These defects, or in this Letter slots, have been placed in InP lasers used for telecommunications applications, around 1.5 µm, and have achieved SMSR>40 dB[14]. Slotted lasers filter out the desired mode by introducing destructive interference to undesired modes in a similar way to DFB lasers but with a different geometry. The slot dimensions are larger and spaced further apart so photolithography can be used to define the patterns, reducing the cost of fabrication. It is easy to monolithically integrate them with other optical components and they have achieved success in widely tunable laser designs used in optical communications[1516].

In this Letter we present a slotted ICL operating in the single-mode CW regime at room temperature emitting in the mid-infrared range at 3.5 µm.

ICL structures were grown with molecular beam epitaxy on n-type GaSb substrates. The bottom cladding layer is a 3.2 µm thick superlattice of AlSb-InAs followed by a 500 nm thick GaSb separate confinement layer (SCL). Two symmetric SCLs surround the active region to increase the index of refraction and improve mode confinement. The active region is realized with 7 interband active stages. Emission occurs in type-II "W" quantum wells (QWs) where a GaInSb hole well is sandwiched between two InAs electron wells to provide good wave function overlap for the optical transition and to help reduce Auger losses[6]. The QWs are surrounded by injectors whose thicknesses and compositions are optimized to transport and balance the carriers throughout the layer and designed to emit around 3.5 µm. The laser is topped with a 1.9 µm thick upper cladding layer.

Fabry-Pérot (FP) ICLs were fabricated with 8 µm mesa ridges and cavities between 1 mm to 2 mm. Lasers with cleaved, uncoated facets were mounted epi-side up on copper heat sinks in order to verify the central emission wavelength and growth quality with respect to multi-mode laser performance. FIG. 1 shows a 1.6 mm long FP ICL operating in CW mode up to 33 °C before the power output drops to below 1 mW. At 20 °C, the threshold current, $I_{th,FP}$, was 55 mA and the thermal rollover point, or maximum power output ($I_{max,FP}, P_{max,FP}$), occurred at 130 mA, 11 mW. The position of the rollover is largely dictated by the thermal management of the mounted device. The multi-mode spectrum in the inset shows a central wavelength around 3.5 µm when the injected current is 100 mA at 20 °C and has a spectral emission envelope approximately 15 nm wide. On average, the wavelength was shifted

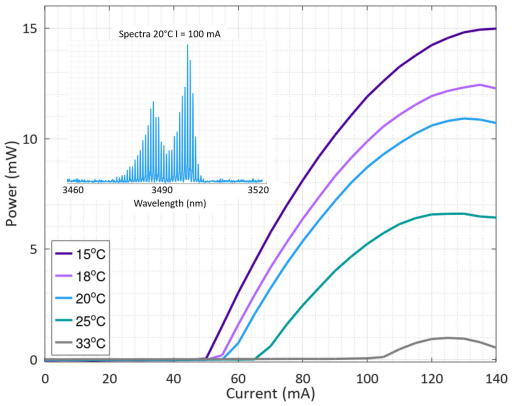

FIG. 1. Typical CW performance of a 1.6 mm long FP ICL around room temperature is presented. The laser operates up to 33 °C mounted epi-side up. The multi-mode spectrum at 20 °C is shown on the inset for injected current of 100 mA.

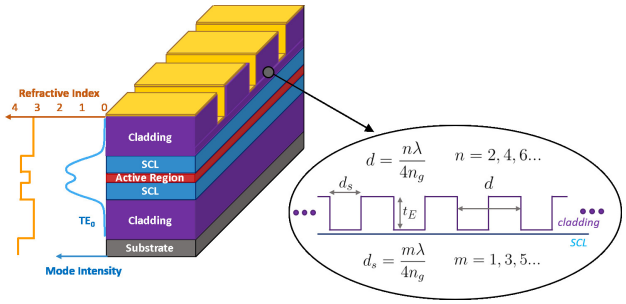

FIG. 2. *Left to right:* The refractive index and mode intensity is plotted for each layer in an ICL's architecture. Next, the cross section of a typical ICL is shown with the slotted waveguide. Finally, key parameters of the slotted waveguide are illustrated, highlighting $d = n\lambda/4n_g$ which provides an intuitive picture on meeting the criteria for constructive vs destructive interference (d vs d_s).

by 0.1 nm mA^{-1} at 20 °C for injected currents approximately halfway between $I_{th,FP}$ and $I_{max,FP}$.

From the FP ICLs spectra, the central wavelength and FWHM were used to design and simulate a slotted waveguide for single-mode emission. An illustration of the structure is shown in FIG. 2. The mesa for the ICLs are defined through the active region up to the bottom cladding to prevent current spreading and improve current injection. The refractive index profile is sketched and the TE_0 mode is plotted for the ICL geometry. When slots are introduced along the length of the laser, the mode is perturbed by the interfaces between the upper cladding and air gaps.

The slot geometry is determined by simulations conducted using FIMMWAVE/FIMMPROP by Photon design, which solve Maxwell's equations using a finite difference eigenmode solver. FIG. 2 illustrates the parameters varied to obtain single-mode operation. This includes the slot spacing (d), the slot width (d_s), the etch depth (t_E), and the number of slots (N)[17]. The slot spacing is used to select the desired lasing wavelength while the slot width determines the amount of loss from the feature. The etch depth controls how much the slots will interact with the tail of the propagating mode leading to an approximately exponential relationship[18]. Normally the number of slots is small for slotted lasers[14] (on the order of 20) and does not span the entire length of the laser, as for a DFB laser.

The refractive index of each layer and its dispersive properties in the epitaxial structure is important to have an accurate value of the effective group index n_g in the simulation. This modelled using the weighted average of the refractive index according to the layer thickness. The simulation assumes the device is passive, though of course the slot placement actually modifies the threshold gain values needed to support each longitudinal cavity mode. The results from the simulation give modulus squared values of the TE_{00} mode reflection and transmission coefficients of the reflectivity peaks supported by the waveguide geometry and defines their position, height, and full width half max (FWHM). The criteria to be single-mode is when one of the reflectivity peaks overlap with a longitudinal cavity mode of the FP ICL and when the FWHM is narrow enough that it only contains one of the cavity modes.

The photolithography system used has a resolution limit of ≈1 µm and imposes a constraint on the design. This resolution depends on the photoresist, thickness, wavelength and quality of surface. Narrower slot widths are difficult to achieve during the dry etching step due to the decreasing aspect ratio (width/depth approximately 1 µm/2 µm). 1.2 µm slots could be achieved and reproduced reliably, so they were selected for the first proof of concept.

In this design slots are placed along the entire length of the laser, meaning the length L and d determine N, to allow more flexibility during fabrication. The ultimate number of slots needed to interact with the propagating cavity mode is constrained by the material choice. The more slots that are needed to have distributed feedback, the longer the laser becomes. This shrinks the cavity mode spacing and neighbouring modes could begin to be supported by the reflectivity peak. The other consideration for the length is how the increase in the amount of gain offered by the material offsets the increase in total losses from additional slots. This is not explicitly simulated here, so the reflectivity strength, R, from the passive structure that yielded a working laser was determined empirically.

FIG. 3 shows how the design affects the reflectivity from the slot pattern. The best performing FP ICLs, with the lowest threshold currents and highest maximum power, are typically between 1 mm to 2 mm long. Since specific values of d are required to align the reflectivity peaks with the FP ICL spectra, a range for N is initially defined. As N increases, the FSR decreases faster than the FWHM of the slots. Therefore, single-mode emission is only likely for shorter lasers where the minimum FWHM is 0.78 nm. The slot depth can be used to independently optimize the FWHM and R of the slot pattern, as shown in FIG. 3(b) for a laser with $N = 298$. The slots should remain in the upper cladding in order to preserve optimal mode confinement and to keep the losses low.

For a slot spacing d =6.68 µm the resulting reflectivity peak spacing was 236 nm. This is well outside the expected spectral envelope width of approximately 15 nm and large enough

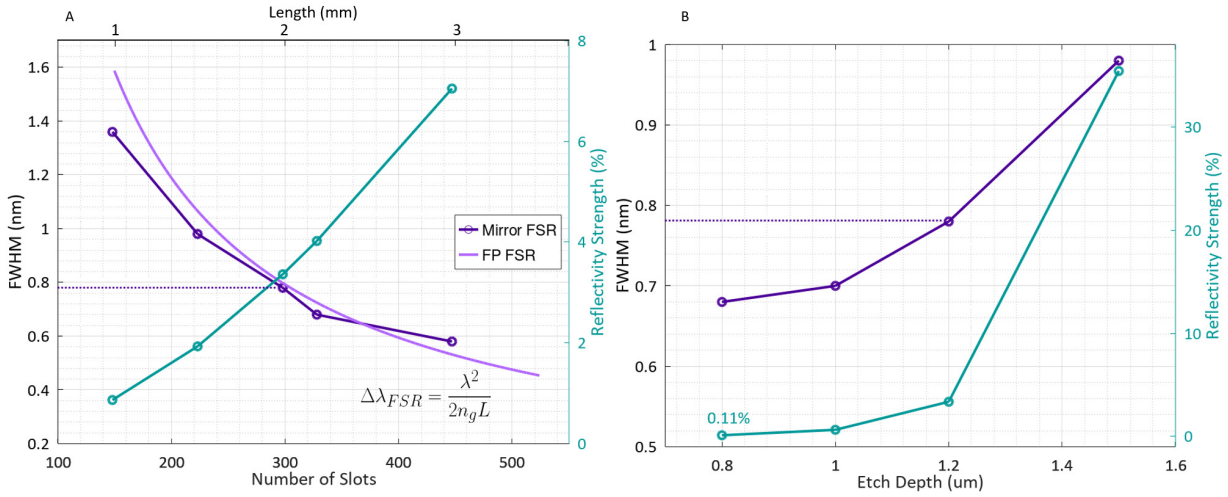

FIG. 3. (a) The cavity mode spacing, FSR, is plotted with the simulated FWHM while changing the total length (equivalently, N). This is done for a slot pattern with d =6.68 µm, d_s =1.2 µm, t_E =1.2 µm,λ =3.5 µm, and n_g =3.8575. The dependence of R and the reflectivty peak FWHM is shown with respect to the number of slots. (b) The dependence of R and the FWHM are shown with respect to t_E for the same slot pattern with N fixed to $N = 298$.

to account for any underestimation from pumping well above threshold. This prevents multiple reflectivity peaks from aligning with different longitudinal cavity modes. Based on these simulations, the criteria for single-mode emission is met for slots with d =6.68 µm, d_s =1.2 µm, t_E <1.2 µm and L <2 mm ($N < 300$).

The fabrication of the slotted ICLs begins with the definition of the slots in order to maximize the resolution from a uniform surface. A Si_3N_4 hard mask is deposited on the ICL sample using plasma enhanced chemical vapour deposition (PECVD) to achieve 1.2 µm resolution. After the hard mask is opened using a fluorine based dry etch, the slot pattern is transferred to the ICL sample using a BCl_3-Ar dry etch. BCl_3-Ar are used in order to keep the slot walls of the AlSb-InAs superlattice cladding smooth[19] and a lowered chamber pressure, with respect to mesa dry etching, is used in an attempt to improve the sidewall angles. The etch depth is a sensitive parameter for the SMSR but cannot be precisely controlled due to small size of the slots, so we can only ensure the etch is in an appropriate range indirectly (≈1 µm).

Next, standard FP ICL fabrication begins[20]. Narrow mesa ridges were fabricated to study CW operation. 8 µm was selected to minimize higher order lateral modes but maximize output power. A thick photoresist was deposited to transfer the mesa pattern to the ICL sample via dry etching. This recipe consisted of BCl_3-Cl_2-Ar in order to etch through the active region to the bottom cladding with a smooth profile. The isolation layer is deposited next and consists of a hardened photoresist with narrow portions on top of the mesa opened for current injection through the metal contacts subsequently deposited. The metal contacts consist of Ti-Au deposited using thermal evaporation. The substrate is then thinned to 200 µm to 250 µm before Pd-GeNiAu is sputtered on for a bottom contact. The Au is diffused through the substrate by briefly heating the sample to 190 °C before lasers of lengths between 1 mm to 2 mm are defined by cleaving facets.

The inset of FIG. 4 shows the cross section of the slots after top contact metal deposition. This procedure resulted in d_s =1.2 µm for an etch depth of t_E =0.8 µm. The development time of the isolation layer needs to be limited to protect the corners of the mesa, preventing shorts, but also enough to clear resist at the very bottom of the slots.

A series of operating conditions were studied in order to understand the range of single-mode operation that could be achieved. The slotted ICL discussed here has slots etched t_E =0.8 µm deep, d_s =1.2 µm wide and with a period of d =6.68 µm. The P-I performance is shown in FIG. 4 for a 1.8 mm long slotted ICL. At 20 °C, I_{th} was 88 mA while $I_{max,Slot}$ and $P_{max,Slot}$ were 140 mA and 2.1 mW, respectively. The spectra from slotted ICLs with different etch depths are included in the Supplementary Material section.

In FIG. 5(a), the spectra at 20 °C and $I = I_{max,Slot}$ is shown to illustrate SMSR≈13 dB could be achieved with this design. In FIG. 5(b), the wavelength tunability is presented over the range where stable single-mode emission and predictable tuning could be expected for $I_{th} < I < I_{max,Slot}$. At 21 °C and 18 °C wavelength tunability of ≈0.1 nm mA^{-1} was measured. For operating conditions at lower temperatures and currents, multi-mode emission could be observed, though with a spectral emission envelope much narrower than for a FP ICL. Potentially the increased heating of the active region helps to suppress the modes near the reflectivity peak or the cavity mode becomes more aligned with the reflectivity peaks of the slots leading to single-mode emission. This is supported by the improvement of SMSR over the injected current range as shown by the inset of FIG. 5(b) at for 21 °C. The SMSR changes from ≈8 dB at 120 mA to ≈12 dB at 139 mA.

The SMSR of this slotted ICL is lower than the industry norm

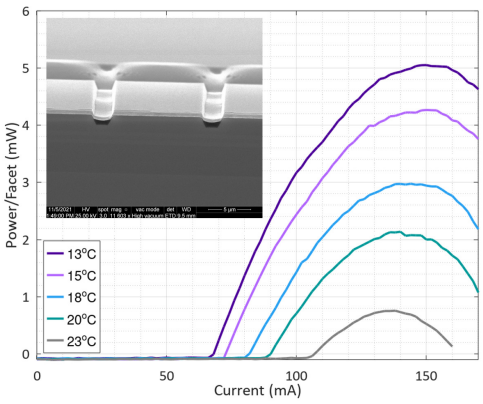

FIG. 4. The P-I curves of a slotted ICL are shown in CW mode as the operating temperature is varied. Operation with power output to around 1 mW is achieved up to 23 °C for a 1.8 mm long laser. The etched slots had t_E =0.8 µm, d_s =1.2 µm, and d =6.68 µm. On the inset, a SEM image of the slot cross section taken from the center of a cleaved 100 µm ridge after Au deposition is depicted. The bottom of the slot is d_s =1.2 µm wide and was etched to a depth of t_E =0.8 µm.

but the measurements reported here used an imaging spectrometer with slits and gratings. Typically, an optical spectrum analyzer is used for these measurements and they include narrow optical filters which improve the dynamic range. The high noise floor is likely due to input coupling issues and scattering from bright modes, reducing the dynamic range possible. Consequently, this means our measurements represent a minimum SMSR of the device.

The material model used for FIMMWAVE simulations has been verified to yield a functional waveguide design. Because the devices fabricated were indeed single-mode, an empirical link to a gain margin given by $R < 1\%$ was established for passive simulations. Now, parameters such as length and total number of slots can be decoupled for a more robust design that can be readily employed across different growths. To extend the range of conditions that yield single-mode emission, the FWHM can be narrowed by etching deeper. The FWHM should be <1.5 nm and the etch depth can be extended from t_E =1 µm to 1.9 µm. The trade off between etch depth and number of slots will be important for the future fabrication of multi-section devices, such as Vernier tuned ICLs, that are planned to further broaden the tuning range.

In conclusion, the initial demonstration of the performance for a single-mode ICL has been presented. Simulations of the waveguide were conducted to determine the best geometry of the slots that were subsequently patterned on ICL mesa ridges using standard UV photolithography and dry etching. Single-mode emission was demonstrated for a 1.8 mm long and 8 µm wide laser in CW mode around 20 °C with a wavelength tunability of 0.1 nm mA^{-1}, a threshold current of 88 mA, and a maximal output power of 2 mW per facet. Even when multi-mode emission was measured, some distributed feedback reduced the number of modes lasing with respect to a FP ICL. The performance we report validates the integration of a slotted waveguide with ICL architecture emitting at λ =3.5 µm.

See the Supplementary Material section for spectra from slotted ICLs with deeper etch depths.

ACKNOWLEDGMENTS

This project is part of the OPTAPHI Training Network and has received funding from the European Union's Horizon 2020 research and innovation programme under the Marie Sklodowska-Curie agreement No. 860808 and the French program on "Investments for the Future" (ANR-11-EQPX-0016).

[1] C. Yao, S. Gao, Y. Wang, P. Wang, W. Jin, and W. Ren, "Mir-pump nir-probe fiber-optic photothermal spectroscopy with background-free first harmonic detection," IEEE Sensors Journal **20**, 12709 (2020).
[2] M. von Edlinger, J. Scheuermann, L. Nählea, C. Zimmermann, L. Hildebrandt, M. Fischer, J. Koeth, R. Weih, S. Höfling, and M. Kamp, "Dfb interband cascade lasers for tunable laser absorption spectroscopy from 3 to 6 um," Proc. of SPIE: Quantum Sensing and Nanophotonic Devices XI , 899318 (2014).
[3] T. Aldhafeeri, M. K. Tran, R. Vrolyk, M. Pope, and M. Fowler, "A review of methane gas detection sensors: Recent developments and future perspectives," Inventions **5**, 28 (2020).
[4] J. Pangerl, M. Muller, T. Ruck, S. Weigl, and R. Bierl, "Characterizing a sensitive compact mid-infrared photoacoustic sensor for methane, ethane and acetylene detection considering changing ambient parameters and bulk composition (n2, o2 and h2o)," Sensors and Actuators: B. Chemical **352**, 130962 (2022).
[5] R. Q. Yang, "Infrared laser based on intersubband transitions in quantum wells," Superlattices and Microstructures **17**, 77 (1995).
[6] J. R. Meyer, W. W. Bewley, C. L. Canedy, C. S. Kim, M. Kim, C. D. Merritt, and I. Vurgaftman, "The interband cascade laser," Photonics **7**, 75 (2020).
[7] I. Vurgaftman, R. Weih, M. Kamp, J. Meyer, C. Canedy, C. Kim, M. Kim, W. Bewley, C. Merritt, J. Abell, and S. Hoefling, "Interband cascade lasers," Journal of Physics D : Applied Physics **48**, 123001 (2015).
[8] L. Cerutti, D. A. Diaz-Thomas, J. B. Rodriguez, M. Rio-Calvo, G. Pariarche, A. N. Baranov, and E. Tournié, "Quantum well interband semiconductor lasers highly tolerant to dislocations," Optica **8**, 1397 (2021).
[9] J. Koeth, R. Weih, J. Scheuermann, M. Fischer, A. Schade, M. Kamp, and S. Hofling, "Mid infrared dfb interband cascade lasers," Proc. of SPIE **10403**, 1040308 (2017).
[10] C. S. Kim, M. Kim, W. W. Bewley, J. R. Lindle, C. L. Canedy, I. Vurgaftman, and J. R. Meyer, "Single-mode distributed-feedback interband cascade laser for the midwave infrared," Applied Physics Letters **88**, 191103 (2006).
[11] Q. Gaimard, L. Cerutti, R. Teissier, and A. Vicet, "Distributed feedback gasb based laser diodes with buried grating," Appl. Phys. Lett. **104**, 161111 (2014).
[12] R. Weih, L. Nahle, S. Hofling, J. Koeth, and M. Kamp, "Single mode interband cascade lasers based on lateral metal gratings," Applied Physics Letters **105**, 071111 (2014).
[13] D. Kozlowski, J. Young, J. England, and R. Plumb, "Longitudinal mode control in 1.3pm fabry-perot lasers by mode suppression," IEEE Proc.-Optoelectron **143**, 71 (1996).
[14] Q. Lu, W. Guo, D. Byrne, and J. Donegan, "Design of slotted single-mode lasers suitable for photonic integration," IEEE Photonics Technology Letters **22**, 787 (2010).
[15] D. C. Byrne, J. P. Engelstaedter, W. Guo, Q. Lu, B. Corbett, B. Roycroft, J. O'Callaghan, F. H. Peters, and J. F. Donegan, "Discretely tunable semiconductor lasers suitable for photonic integration," IEEE Quantum Electronics **15**, 482 (2009).
[16] M. Nawrocka, Q. Lu, W. Guo, A. Abdullaev, F. Bello, J. O'Callaghan, T. Cathcart, and J. F. Donegan, "Widely tunable six-section semiconductor laser based on etched slots," Optics Express **22**, 18949 (2014).
[17] J. Patchell, D. Jones, B. Kelly, and J. O'Gorman, "Specifying the wavelength and temperature tuning range of a fabry perot laser containing refractive index perturbations," Proc. of SPIE: Opto-Ireland 2005 **5825**, 1 (2005).

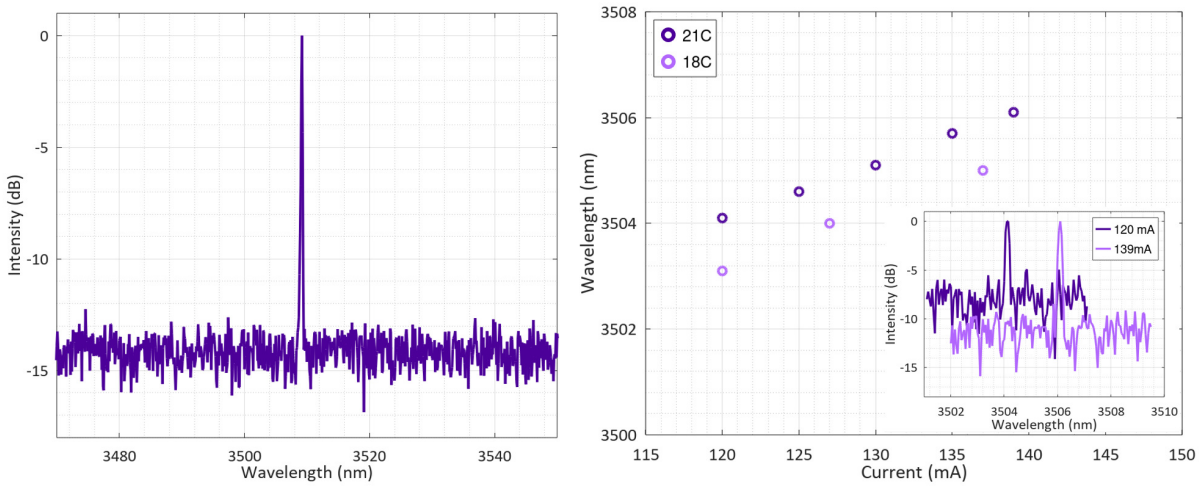

FIG. 5. (a) The spectra for the slotted ICL at 20 °C and $I = I_{max,Slot}$ is plotted. (b) The wavelength tuning for $I_{th} < I < I_{max,Slot}$ at two different temperatures is plotted for when single-mode emission was achieved. The inset depicts spectra at 21 °C for the start and end of the wavelength tuning range.

[18] J. P. Englestadter, *Laser Diodes for Photonic Integrated Circuits*, Ph.D. thesis, University College Cork (2009).

[19] S. S. Cooperman, H. K. Choi, H. H. Sawin, and D. F. Kolesar, "Reactive ion etching of gaas and algaas in a bcl3–ar discharge," Journal of Vacuum Science and Technology B **7**, 41 (1989).

[20] D. A. Diaz-Thomas, O. Stepanenko, M. Bahriz, S.Calvez, E. Tournié, A. N. Baranov, G. Almuneau, and L. Cerutti, "Interband cascade lasers with algaassb cladding layers emitting at 3.3 um," Optics Express **27**, 31425 (2019).